BRAIN
ORIGINAL ARTICLE

CAPRIN1 haploinsufficiency causes a neurodevelopmental disorder with language impairment, ADHD and ASD

Lisa Pavinato,[1,2] Andrea Delle Vedove,[2,3] Diana Carli,[4,5] Marta Ferrero,[1,6] Silvia Carestiato,[1] Jennifer L. Howe,[7] Emanuele Agolini,[8] Domenico A. Coviello,[9] Ingrid van de Laar,[10] Ping Yee Billie Au,[11] Eleonora Di Gregorio,[12] Alessandra Fabbiani,[13,14,15] Susanna Croci,[14,15] Maria Antonietta Mencarelli,[13] Lucia P. Bruno,[14,15] Alessandra Renieri,[13,14,15] Danai Veltra,[16] Christalena Sofocleous,[16] Laurence Faivre,[17,18] Benoit Mazel,[17] Hana Safraou,[18,19] Anne-Sophie Denommé-Pichon,[18,19] Marjon A. van Slegtenhorst,[10] Noor Giesbertz,[20] Richard H. van Jaarsveld,[20] Anna Childers,[21] R. Curtis Rogers,[21] Antonio Novelli,[8] Silvia De Rubeis,[22,23,24,25] Joseph D. Buxbaum,[22,23,24,26] Stephen W. Scherer,[27,28] Giovanni Battista Ferrero,[29] Brunhilde Wirth[2,3,†] and Alfredo Brusco[1,12,†]

[†]These authors contributed equally to this work.

We describe an autosomal dominant disorder associated with loss-of-function variants in the Cell cycle associated protein 1 (*CAPRIN1*; MIM*601178). *CAPRIN1* encodes a ubiquitous protein that regulates the transport and translation of neuronal mRNAs critical for synaptic plasticity, as well as mRNAs encoding proteins important for cell proliferation and migration in multiple cell types. We identified 12 cases with loss-of-function *CAPRIN1* variants, and a neurodevelopmental phenotype characterized by language impairment/speech delay (100%), intellectual disability (83%), attention deficit hyperactivity disorder (82%) and autism spectrum disorder (67%). Affected individuals also had respiratory problems (50%), limb/skeletal anomalies (50%), developmental delay (42%) feeding difficulties (33%), seizures (33%) and ophthalmologic problems (33%).

In patient-derived lymphoblasts and fibroblasts, we showed a monoallelic expression of the wild-type allele, and a reduction of the transcript and protein compatible with a half dose. To further study pathogenic mechanisms, we generated s*CAPRIN1*$^{+/-}$ human induced pluripotent stem cells via CRISPR–Cas9 mutagenesis and differentiated them into neuronal progenitor cells and cortical neurons. *CAPRIN1* loss caused reduced neuronal processes, overall disruption of the neuronal organization and an increased neuronal degeneration. We also observed an alteration of mRNA translation in *CAPRIN1*$^{+/-}$ neurons, compatible with its suggested function as translational inhibitor. *CAPRIN1*$^{+/-}$ neurons also showed an impaired calcium signalling and increased oxidative stress, two mechanisms that may directly affect neuronal networks development, maintenance and function. According to what was previously observed in the mouse model, measurements of activity in *CAPRIN1*$^{+/-}$ neurons via micro-electrode arrays indicated lower spike rates and bursts, with an overall reduced activity. In conclusion, we demonstrate that *CAPRIN1* haploinsufficiency causes a novel autosomal dominant neurodevelopmental disorder and identify morphological and functional alterations associated with this disorder in human neuronal models.

1 Department of Medical Sciences, University of Turin, 10126 Turin, Italy
2 Institute of Human Genetics, Center for Molecular Medicine Cologne, Center for Rare Diseases Cologne, University Hospital Cologne, University of Cologne, 50931 Cologne, Germany

Received February 14, 2022. Revised July 04, 2022. Accepted July 11, 2022. Advance access publication July 27, 2022

3 Institute for Genetics, University of Cologne, 50674 Cologne, Germany
4 Department of Public Health and Pediatrics, University of Turin, 10126 Turin, Italy
5 Pediatric Onco-Hematology, Stem Cell Transplantation and Cell Therapy Division, Regina Margherita Children's Hospital, Città Della Salute e Della Scienza di Torino, 10126 Turin, Italy
6 Experimental Zooprophylactic Institute of Piedmont, Liguria e Valle d'Aosta, 10154 Turin, Italy
7 The Centre for Applied Genomics, Genetics and Genome Biology Program, The Hospital for Sick Children, Toronto, ON M5G 0A4, Canada
8 Laboratory of Medical Genetics, IRCCS, Ospedale Pediatrico Bambino Gesù, Rome, Italy
9 Laboratory of Human Genetics, IRCCS Istituto Giannina Gaslini, 16147 Genoa, Italy
10 Clinical Genetics, Department of Clinical Genetics, Erasmus MC, University Medical Center Rotterdam, 3015 CN, Rotterdam, The Netherlands
11 Department of Medical Genetics, Alberta Children's Hospital Research Institute, University of Calgary, Calgary, AB T2N 1N4, Canada
12 Medical Genetics Unit, Città della Salute e della Scienza University Hospital, 10126 Turin, Italy
13 Medical Genetics Unit, Azienda Ospedaliera Universitaria Senese, 53100 Siena, Italy
14 Medical Genetics, University of Siena, 53100 Siena, Italy
15 Med Biotech Hub and Competence Center, Department of Medical Biotechnologies, University of Siena, 53100 Siena, Italy
16 Laboratory of Medical Genetics, School of Medicine, National & Kapodistrian University of Athens, 'Aghia Sophia' Children's Hospital, 11527 Athens, Greece
17 Centre de référence Anomalies du Développement et Syndromes Malformatifs, Fédération Hospitalo-Universitaire TRANSLAD, CHU Dijon, 21079 Dijon, France
18 UMR1231 GAD, Inserm—Université Bourgogne-Franche Comté, 21078 Dijon, France
19 Unité Fonctionnelle Innovation en Diagnostic génomique des maladies rares, FHU TRANSLAD, CHU Dijon Bourgogne, 21000 Dijon, France
20 Department of Genetics, University Medical Centre Utrecht, 3584 CX, Utrecht, The Netherlands
21 Greenwood Genetic Center, Greenville, SC 29646, USA
22 Seaver Autism Center for Research and Treatment, Icahn School of Medicine at Mount Sinai, New York, NY 10029, USA
23 Department of Psychiatry, Icahn School of Medicine at Mount Sinai, New York, NY 10029, USA
24 The Mindich Child Health and Development Institute, Icahn School of Medicine at Mount Sinai, New York, NY 10029, USA
25 Friedman Brain Institute, Icahn School of Medicine at Mount Sinai, New York, NY 10029, USA
26 Department of Neuroscience, Icahn School of Medicine at Mount Sinai, New York, NY 10029, USA
27 Department of Molecular Genetics, University of Toronto, Toronto, ON M5S 1A8, Canada
28 McLaughlin Centre, University of Toronto, Toronto, ON M5S 1A1, Canada
29 Department of Clinical and Biological Sciences, University of Turin, 10149 Orbassano, TO, Italy

Correspondence to: Professor Alfredo Brusco, PhD
Department of Medical Sciences
University of Turin via Santena 19, 10126 Turin, Italy
E-mail: alfredo.brusco@unito.it

Keywords: CAPRIN1; neurodevelopment; RNG105; ADHD; ASD

Introduction

The cell cycle Associated PRote IN 1 (*CAPRIN1*; MIM*601178) gene encodes an RNA-binding protein that is ubiquitous and is highly expressed in the brain (Supplementary Fig. 2A). While it is mainly known for its role in cancer,[1] evidence implicating CAPRIN1 in brain development and function is emerging from animal studies. Homozygous *Caprin1* knock-out mice (*Caprin1*$^{-/-}$) are not viable due to respiratory failure after birth.[2] *Caprin1* haploinsufficient mice (*Caprin*$^{+/-}$) show reduced sociability, attenuated preference for social novelty or novel objects, and deficits in reversal learning compared to controls.[3] Further, *Caprin1* deficiency in neurons causes a reduction of the complexity of the dendritic arborization and smaller dendritic spines, leading to reduced postsynaptic response to stimulation, and impaired long-term memory.[2,4] Molecularly, *Caprin1* deficiency in neurons causes altered localization of a subset of mRNAs encoding proteins fundamental for synaptic plasticity, including AMPA (α-amino-3-hydroxy-5-methyl-4-isoxazolepropionic acid) receptors.[4,5]

CAPRIN1 interacts with two other RNA-binding proteins critical for the formation of ribonucleoparticles (RNP) known as RNA granules: Fragile-X Mental Retardation Protein (FMRP)[5] and G3BP1.[6,7] Moreover, CAPRIN1 is suggested to be a scaffold protein able to mediate the formation of distinct RNP complexes.[6] CAPRIN1 localizes in neuronal RNA granules at dendrites,[4,8] where it binds key mRNAs involved in neuronal activity and synaptic plasticity, such as CAMK2A, BDNF, CREB, MAP2 and TRKB.[8] Following synaptic stimulations, CAPRIN1 can repress mRNA local translation through its N-terminal domain.[8] Nevertheless, the overexpression of CAPRIN1 results in a global inhibition in protein synthesis, through the phosphorylation of eukaryotic translation initiation factor 2 alpha (ELF2A).[9]

Previous exome-wide screenings in neurodevelopmental disorders have identified a few cases with nonsense variants in *CAPRIN1*,[10,11] suggesting that the gene might be a candidate risk gene for autism spectrum disorder (ASD). Also, in a recent integrated analysis on over 63 000 exomes (over 20 000 with ASD),[12] *CAPRIN1* was identified as one of the 183 genes associated with ASD, with a false discovery rate (FDR) ≤ 0.05 (*CAPRIN1* TADA-ASD FDR = 0.01). Interestingly, the association of the gene with a broader spectrum of neurodevelopmental disorders (NDDs) was even stronger (*CAPRIN1* TADA-NDD FDR = 0.00065) and *CAPRIN1* was listed among the 373 genes associated with general NDDs.[12]

Here, we integrate human genetic data and functional evidence on patient-derived cells and human neuronal models to describe a novel autosomal dominant neurodevelopmental disorder associated with *CAPRIN1* haploinsufficiency.

Materials and methods

Exome and genome sequencing, variant calling and prioritization

We identified *CAPRIN1* variants in clinical diagnostic or research settings by exome sequencing, genome sequencing or array CGH (60 K; Agilent Technologies) (see Supplementary material). Exome sequencing or genome sequencing trio raw data were processed and analysed using in-house implemented pipelines. High-quality variants were filtered against public databases (dbSNP150 and gnomAD v.2.1.1) so that only variants with unknown frequency or with a minimum allele frequency (MAF) < 0.1% were considered. A further variant stratification in conformity with the American College of Medical Genetics and Genomics (ACMG) guideline,[13] also considering mode of inheritance and functional *in silico* prediction of impact, allowed us to consider the final set of variants for possible associations with the phenotype. All the variants are referred to genome assembly GRCh37 (hg19), NM_005898.5.

Informed consent was obtained from the participating families and the study protocol was approved by each institutes internal Ethics Committees, according to the Declaration of Helsinki.

Cell cultures

Peripheral blood mononuclear cells (PBMCs) were isolated from whole blood using Histopaque-1077 (Sigma-Aldrich) and subsequently immortalized with Epstein–Barr virus. The resultant lymphoblastoid cell line (LCL) was cultured in Roswell Park Memorial Institute medium (Gibco, Thermo Fisher Scientific) supplemented with 1% Pen-Strep and 1% L-glutamine. Fibroblasts were obtained from a skin biopsy and cultured in Dulbecco's modified Eagle medium supplemented with 10% foetal bovine serum (FBS), 1% Pen-Strep and 1 mM sodium pyruvate (Thermo Fisher Scientific) at 37°C, 5% CO_2.

DNA and RNA extraction and analysis

DNA extraction from cells was performed by incubating cell pellets in buffer supplemented with proteinase K (DNeasy Blood & Tissue Kit; Qiagen) for 90 min at 60°C, followed by 10 min at 95°C. After centrifugation at 14 000 rpm for 10 min, the supernatant was recovered and incubated for 30 min at 37°C and subsequently quantified at NanoDrop (Thermo Fisher Scientific).

Total RNA was extracted from fibroblasts, PBMCs or LCL using the Direct-Zol RNA MiniPrep system (Zymo Research); genomic DNA was removed by treatment with DNase I (Sigma-Aldrich), following the manufacturer's protocol. To evaluate gene expression in different tissues, commercially available total RNA from foetal total brain and adult total cerebellum, brain, frontal cortex, placenta, kidney, stomach, heart and lung were used (Applied Biosystems, Thermo Fisher Scientific).

The M-MLV Reverse Transcriptase kit (Invitrogen, Thermo Fisher Scientific) was used to generate cDNA. Expression of *CAPRIN1* was measured using the Universal Probe Library system (probe #67, Roche Diagnostics) and two specific intron-spanning primers. Reference genes *TBP* and *GUSB* were measured with human predesigned assays (Applied Biosystems, Thermo Fisher Scientific). Reactions were carried out in triplicate on an ABI 7500 real-time PCR machine using the ABI 2X TaqMan Universal PCR Master Mix II, according to the manufacturer's instructions (Thermo Fisher Scientific).

Analysis of splicing variants

Total RNA was extracted from LCLs, and reverse transcribed as described before; cDNA was amplified with touchdown PCR using KAPA Taq PCR Kit (Roche Diagnostics). Amplimers were visualized into 2% TBE-agarose gel using ChemiDoc Imaging System (Bio-Rad). Bands were gel-excised, and the DNA extracted with a GenElute Gel Extraction Kit (Sigma-Aldrich). Fragments were sequenced using the Sanger method.

Evaluation of nonsense-mediated decay

A total of 9×10^4 fibroblasts from Cases 8 and 9 were seeded in six-well plates and cultured until 80% confluence. From Case 3, 6×10^5 lymphoblastoid cells were used. Cells were then treated with 100 μg/ml cycloheximide (CHX) for 6 h. After washing with 1× PBS, cells were detached with 1× Trypsin (Gibco) and prepared for RNA extraction. The Sanger method was used to sequence cDNAs.

CRISPR–Cas9 heterozygous *CAPRIN1* knock-out generation

Human induced pluripotent stem cells (hiPSCs) derived from human umbilical vein endothelial cells (HUVEC)[14] were used to generate an isogenic hiPSC line carrying a heterozygous *CAPRIN1* deletion based on a published protocol.[15] Briefly, HUVEC hiPSCs were cultured in mTeSR Plus medium (StemCell Technologies) supplemented with 10 μM Y-27632 (Selleckchem) at a confluence of 2×10^4 cells/cm^2. After 48 h, cells were transfected with FuGENE HD Transfection Reagent (Promega) with a Cas9 expression vector (pX330-hCas9-long-chimeric-grna-g 2p) in which a *CAPRIN1*-targeting gRNA (5′-ACCGTTTGCATGGATTGGAA-3′) was subcloned. Starting 24 h post-transfection, the cells were selected for 48 h with 1 μg/ml puromycin (ThermoFisher Scientific) and allowed to recover for 24 h, before being split with Accutase (ThermoFisher Scientific) and seeded in mTeSR Plus medium with 10 μM Y-27632 into a 96-well plate at single cell density. After 12 days, colonies were split into 24-well plates. When ready for passaging, cells were divided into two aliquots: one was frozen and the other used for DNA extraction with QuickExtract DNA Extraction Solution (Lucigen). A 326-bp region targeted by the gRNA was amplified by PCR (CAPRIN1-SA_F1: 5′-TCCCTTCCTGCTGCGTCTCA-3′; CAPRIN1-SA_R1: 5′-ACAGGCACATCACTCATAAGGCTAA-3′) and genome editing was screened with a T7 Endonuclease (NEB) assay.

In the case of a positive result, a 901-bp region was sequenced by Sanger sequencing (CAPRIN1-E14_F1: 5′-TCATCCACAAGTGAG GGGTACACA-3′; CAPRIN1-E14_R1: 5′-AGGTGCTTGCTCAAGAATC AAGGTA-3′). Clones harbouring heterozygous loss-of-function (LoF) variants were expanded for further studies and are referred as *CAPRIN1*$^{+/-}$, while wild-type cells are referred to as CTRL.

Human induced pluripotent stem cell differentiation into cortical neurons

Human induced pluripotent stem cells were differentiated into cortical neurons as previously described[6,17] with some modifications. Briefly, hiPSCs were grown as usual until confluence. A chess pattern was created using a needle that had squares of 2–3 mm/each; subsequently, they were washed with PBS and left in collagenase (3 mg/ml) for ∼30 min. Detached cells were then gently resuspended into Neuronal Induction Medium #1 (see Supplementary material) and kept in a 5% CO_2 incubator with 35 rpm shaking for 10 days. The medium was changed every other day. At Day 10, embryoid bodies were plated on poly-Ornhitin/Laminin coated plates in Neuronal Induction Medium #2 (Supplementary material) and the medium was changed every other day until confluence. Then, cells were detached and frozen or plated for neuronal differentiation (ND) in PEI/Laminin coated plates with ND medium (see details in Supplementary material). Cells were fed every 3 days, changing half of the medium (for a detailed description, see Supplementary material).

Western blot

Total proteins were extracted from a cellular pellet with RIPA buffer (50 mM Tris-HCl pH 7.5; 150 mM NaCl; 1% NP-40; 0.5% sodium deoxycholate) supplemented with DTT 0.1 M, EDTA 0.5 M and 100× Halt Protease and Phosphatase Inhibitor Cocktail (Thermo Fisher Scientific). Ten micrograms of proteins were diluted into 4× LDS sample buffer and 10× Sample Reducing Agent, and were electrophoresed on 4–12% Bis-Tris Protein Gels (Thermo Fisher Scientific).

Nitrocellulose membranes 0.45 µm were stained with a MemCode Reversible Protein Stain Kit (Thermo Fisher Scientific) and immunoblotted. Antibodies are listed in the Supplementary material. Images were acquired with a ChemiDoc Imaging System and analysed with ImageLab software (BioRad), using volume tools quantification with the global subtraction method. The CAPRIN1 protein level was normalized on Vinculin (MemCode normalization gave similar results).

Immunofluorescence and imaging

When not otherwise stated, immunofluorescence of hiPSC-derived neurons was performed using our standard protocol. Briefly, neurons were plated on coverslips at low confluence (50 000 cells/cm^2). The fixation was performed with 4% PFA 4% sucrose at room temperature for 15 min, followed by three washes for 5 min each with PBS. Coverslips were then stored at 4°C until immunostaining or immediately processed. Cells were permeabilized using PBS 0.1% Triton for 5 min and blocked with PBS 5% BSA for 30 min at room temperature. Primary antibodies were diluted in PBS 1% BSA and left overnight at 4°C; secondary antibodies were diluted in PBS 1% BSA and left for 2 h at room temperature protected from light. A full list of antibodies is given in the Supplementary material. For some experiments, cells were subsequently stained with Phalloidin for 45 min before being mounted with Fluoromount G with 4′,6-diamidino-2-phenylindole (DAPI, Invitrogen). When not otherwise stated, images were acquired using a Zeiss Imager M2 microscope, with or without the Zeiss Apotome grid, and analysed using Fiji/ImageJ.

Calcium recording

Neuronal progenitors from three independent differentiations were plated on coverslips in a six-well plate (50 000 cells/cm^2), in 2 ml of ND medium, and they were cultured for 10 or 14 days. The day of the recording, coverslips were moved to microscope chambers and 0.5 µl F-127 (0.2%) and 0.5 µl of Fluo-4 (Invitrogen) (2 µM) were added in 250 µl of preconditioned medium. After 25 min of incubation (5% CO_2, 37°C), the medium was removed, cells were washed with PBS and 500 µl of preconditioned medium without F-127 and Fluo-4 were added. Coverslips were immediately analysed using a Leica Thunder Microscope (5% CO_2, 37°C) at ×20 plan magnification. Each analysed segment of the coverslip was recorded for 2 min using live imaging. At least 446 cells/genotype and three recordings were analysed using Fiji/ImageJ and summing the IntDen signal of each frame normalized on the lowest IntDen (F_0) of each cell, as previously described.[18]

Reactive oxygen species analysis

Reactive oxygen species (ROS) were detected using the fluorogenic probe CellROX Green Reagent (Thermo Fisher Scientific). Eighteen days after starting the ND (cells plated on coverslips, 50 000 cells/cm^2), 0.5 µl of reagent were added to 250 µl of preconditioned medium. After 30 min of incubation (5% CO_2, 37°C), medium was removed and cells were washed three times with PBS before being fixed with 4% PFA 4% sucrose for 15 min at room temperature. Cells were then washed three times with PBS and once with water, and mounted with Fluoromount G with DAPI (Invitrogen); ×20 images were acquired using a Zeiss Imager M2 microscope within 24 h of the experiment. Analysis was performed using Fiji/ImageJ, setting regions of interest on the DAPI signal (channel 1) and measuring IntDen on the CellROX signal (channel 2). Signals were normalized on the average IntDen of backgrounds. Twenty-one images/genotype were analysed for a total of a minimum of 697 cells/genotype.

Surface Sensing of Translation

Protein synthesis was measured by Surface Sensing of Translation (SUnSET) assay.[19] Differentiated neurons (post-ND Days 4 and 14) were incubated with 1 µM puromycin for 30 min. Puromycin labelled peptides were detected by western blotting or immunostaining using an anti-puromycin antibody. For western blotting, puromycin intensity was normalized on β-actin and on stain free gel activation signal (ChemiDoc Imaging System, 5 min, faint bands): the latter being performed after the electrophoresis and before the transfer. Signal intensities were analysed using BioRad ImageLab software, quantifying the whole lane for anti-puromycin and stain free gel activation signal and the single bands for anti-β-actin (Supplementary Fig. 8B). Similar results were obtained for puromycin normalized on the stain free gel activation signal and β-actin signal.

For immunostaining, images were captured with a Zeiss Imager M2 and analysed using Fiji/ImageJ. The lookup table (LUT) 'royal' was used to better visualize signal intensities; puromycin grey values were registered along the dendrite of six different neurons from 0 to 50 µm in distance from the soma. Bins of 10 µm/each,

starting from 5 µm of distance from the soma, were then generated and the mean intensity of each bin was used for statistical analysis.

Micro-electrode array

Recordings were performed using a multi-electrode array (Multi Channel Systems) at different time points, using a 24-well plate (12 gold electrodes on epoxy material per well). Then 75 000 cells/well were plated on a PEI/Laminin coating. Measurements were done before the medium was changed. Data acquisition and analysis was performed through the Multi-Channel Suite software (Multi Channel Systems), setting the threshold for spike detection at ±10 µV and a band-pass filter with 100 and 3 kHz cut-off frequencies. Spike detection was performed using an adaptive threshold set to 5.5 times the standard deviation of the estimated noise on each electrode. Each plate first rested for 2 min in the recorder. Experiments were performed in a non-humidified incubator at 37°C, recording for 2 min. Neurons from three independent differentiation batches were measured [CTRL $n = 14$ wells (two biological replicates, five technical replicates/each and one biological replicate with four technical replicates); *CAPRIN1*$^{+/-}$ $n = 9$ wells (three biological replicates, three technical replicates/each)].

Statistical analysis

For each experiment, biological triplicates with at least two technical replicates were performed. Except where otherwise indicated, data were analysed with Prism-GraphPad Software performing a Student *t*-test with Welch's correction; *P*-values were indicated as follows: not significant (ns) = $P > 0.05$; *$P \leq 0.05$; **$P \leq 0.01$; ***$P \leq 0.001$; ****$P \leq 0.0001$.

In silico protein structure modelling

CAPRIN1 protein was modelled using Protein Homology/analogY Recognition Engine version 2,[20] choosing the intensive modelling mode option. A pdb file was generated for both wild-type and mutant protein carrying the c.279+1G>T variant and imported in EzMol[21] interface server (v.2.1); the colour code was generated from EzMol, and it was based on the isoelectric point (red: high/positive, white: neutral/zero; blue: low/negative). The resulting image was used to visualize the 3D protein conformation. ClusPro[22–25] protein–protein docking server was used to analyse dimer formation.

Data availability

The data that support the findings of this study are available from the corresponding author, upon reasonable request.

Results

CAPRIN1 variants and patients' clinics

A *de novo* ~1.4 Mb deletion encompassing *CAPRIN1* was detected in a routine diagnostic array CGH screening for patients with neurodevelopmental disorders (Fig. 1A).

The deletion spans eight genes, including *CAPRIN1*. *CAPRIN1* was the only one predicted to be haploinsufficient (gnomAD v.2.1.1, pLI score = 0.97)[26] and had previous evidence of variants in individuals diagnosed with neurodevelopmental disorders.[10–12] Using GeneMatcher[27] and MSSNG databases, we identified by exome or genome sequencing 11 additional cases with nonsense or splicing variants affecting donor/acceptor sites in *CAPRIN1* (Fig. 1A, Table 1 and Supplementary Fig. 1). A nonsense variant identified in Case 9 was paternally inherited and the father was also affected (Case 10). All other variants but one (Case 2) were *de novo*, absent in the control population (gnomAD v.2.1.1) and classified as pathogenic using the ACMG guidelines.[13,28] Two additional cases with LoF variants in *CAPRIN1* were already reported in the literature in large genetic screenings of patients diagnosed with ASD[10,11] (Fig. 1A).

The age of cases ranged from 3 to 48 years old, and all received a clinical diagnosis of neurodevelopmental disorder. Six were born at term with normal parameters after uneventful pregnancies and delivery. Respiratory concerns were reported in six cases, and included foetal respiratory distress, post-natal saturation dips, obstructive sleep apnoea, sudden chocking spells and asthma (Table 1).

An overall representation of *CAPRIN1*-associated phenotypes is shown in Fig. 1B. Language impairment was observed in all cases, with most cases speaking very few words at the last evaluations. Some of the affected individuals were supported with specific tools, such as Case 1, who was helped using a personal picture agenda (Supplementary Video 1). Stereotyped movements and behaviours were also observed in some of the patients (Supplementary Video 2, Case 1).

Intellectual and/or learning disabilities from mild to very severe were reported for all but Cases 1 and 6; ASD was diagnosed in eight patients (67%). Nine of eleven patients (82%) met the diagnostic criteria for attention deficit hyperactivity disorder (ADHD). Four patients had epileptic seizures with different severity: Cases 2 and 4 showed absence type seizures, which resolved after oxcarbazepine and ADHD treatment, respectively. Case 11 had infantile spams beginning at 9 months of age, which became absence epilepsy (Supplementary Video 3) at the last evaluation, and was treated with sodium valproate and carbamazepine. Case 12 suffered from secondary generalized epileptic seizures during sleep, and was treated with valproate with discrete control. Six patients also showed mild skeletal limb malformations, with fifth digit clinodactyly as the prevalent feature (Supplementary Fig. 2B); two patients had scoliosis and mild kyphoscoliosis. Brain MRI was available for six patients, and all the identified anomalies were considered without clinical significance (Supplementary Fig. 2C). Gastrointestinal issues (2/12), feeding difficulties (2/12) and ocular anomalies (4/12) were reported; no facial dysmorphism was evident, although some features, such as broad nasal tip, low hanging columella and thin lip recurred in different cases (Fig. 1C, Supplementary Fig. 2B and Supplementary Table 1). Notably, mild hearing loss has been observed in Cases 3 and 10. This finding supports the recent evidence that lack of *Caprin1* in inner ear is related to progressive hearing loss and reduced recovery from noise exposure in mice.[29] A summary of the prevalent features is reported in Table 1 and a detailed clinical description is available in the Supplementary material.

CAPRIN1 expression and splicing analysis

To verify the consequences of the variants on *CAPRIN1* expression, we measured *CAPRIN1* mRNA levels by quantitative PCR with reverse transcription (RT-qPCR) in fibroblasts and PBMCs from patients, and found that it was reduced, compatible with the loss of one functional allele (Fig. 2A). In Cases 8 and 12, we detected the exclusive expression of the reference allele by Sanger sequencing. To investigate the occurrence of nonsense-mediated decay (NMD) for premature stop codons, we treated fibroblasts with CHX and showed a partial rescue in the expression of the mutant allele by Sanger sequencing

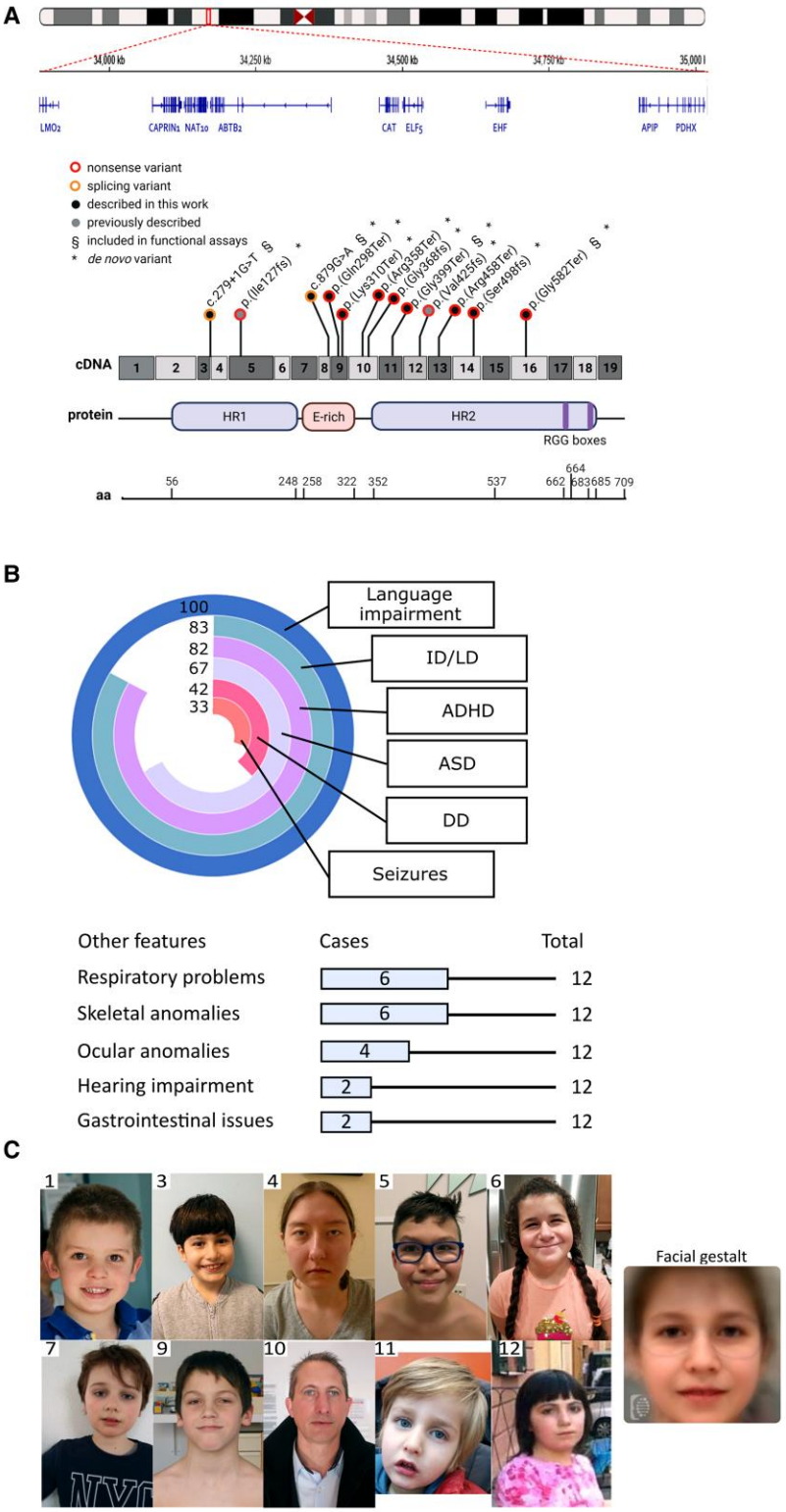

Figure 1 *CAPRIN1*-associated disease: variants and clinical features. (**A**) Schematic representation of a large ~1.4 Mb deletion spanning the *CAPRIN1* gene (*top*) and 11 *CAPRIN1* (NM_005898.5) loss of function variants (*bottom*); 10 single nucleotide variants detected in this work and two variants reported in the literature[10,11] are represented on a schematic view of the protein (created with BioRender.com). Overall, they include two splicing (c.279+1G>T; c.879G>A) and 10 nonsense/frameshift changes. CAPRIN1 structure was schematized according to Wu *et al.*[6]: two highly conserved homologous regions (HR1, 56–248 amino acids and HR2, 352–685 amino acids) and a less conserved glutamate-rich (E-rich) region in between are shown. Moreover, C-terminal Arg-Gly-Gly (RGG) motifs—characteristic of some RNA-binding proteins[6]—are indicated in purple. (**B**) Main neurological (*top*) and non-neurological (*bottom*) features of *CAPRIN1*-associated disease in the 12 cases described here. (**C**) Facial features of the 12 cases do not show peculiar dysmorphisms, although broad nasal tip, low-hanging columella and thin upper lip vermilion seemed recurrent. Facial features analysis by Face2Gene software (FDNA Inc., https://www.face2gene.com/)[56] does not show a peculiar overlap. Further details are provided in Supplementary Fig. 2 and Supplementary Table 1.

Table 1 Clinical features of *CAPRIN1* patients (GenBank: NM_005898.5)

Case	1	2	3	4	5	6	7	8	9	10	11	12
Sex	M	M	M	F	M	F	M	M	M	M	M	F
Age at examination, years	7	12	6	17	10	8	7	7	12	48	3	10
Language impairment	+	+	+	+	+	+	+	+	+	+	+	+
ASD	+	+	+	+	+	–	+	+	–	–	+	–
ID/LD	–	++	+	+	++	–	+++	+	++	+	+	+++
ADHD	+	+	–	+	+	+	NA	+	+	+	–	+
Developmental delay	–	+	+	–	+/–	–	–	–	+	–	+	–
Other behavioural features	+	–	–	+	–	+	–	–	+	+	+	+
Seizures	–	+	–	+	–	–	–	–	–	–	+	+
EEG anomalies	NA	+	–	–	–	NA	NA	NA	NA	NA	+	+
Hands and feet malformations	–	+	+	+	+	–	–	–	+	–	–	+
Breathing problems	–	–	–	+	+	+	–	+	+	+	–	–
Ocular problems	–	–	–	+	+	–	–	–	+	+	–	–
Hearing problems	–	–	+	+	–	–	–	–	–	+	–	–

(+) = Reported in the patient; for ID/LD: + mild; ++ moderate; +++ severe. (–) = not reported in the patient. NA = the information is not available. ADHD = attention deficit hyperactivity disorder; F = female; ID = intellectual disability; LD = learning disability; M = male.

(Fig. 2B). We confirmed a significant reduction of CAPRIN1 protein in fibroblasts derived from patients by western blot (Fig. 2C).

In Cases 2 and 3, the c.279+1G>T and c.879G>A variants were predicted to alter the donor splice sites, since they are at the first nucleotide of intron 3 and at the last base of exon 8.[30] Analysis of the cDNA showed skipping of exon 3 for c.279+1G>T and of exon 8 for c.879G>A (Fig. 2D). In the first case, the mature mRNA is predicted to encode a protein with an in-frame deletion of 31 amino acids (63 bp) occurring in a highly conserved region. Although the specific function of the encoded region is unknown (amino acids 73–93), it falls within the HR1 domain of CAPRIN1 (amino acids 56–248), which partially overlaps with the homodimerization domain (amino acids 132–251). The large concave negatively charged surface formed is a protein–protein binding pocket and it mediates the interaction with up to two molecules of FMRP.[6] *In silico* analysis of mutant protein (CAPRIN1 lacking exon 3) showed an alteration in both its tridimensional structure and its ability to homodimerize (Supplementary Fig. 3B). This could reduce protein stability and thus lead to the reduced abundance that we observed (Supplementary Fig. 3A).

The c.879G>A variant causes the loss of 53 nucleotides, resulting in an out-of-frame protein. Treatment of patient cells with CHX restored a partial expression of the mutant allele, suggesting that it undergoes NMD (Fig. 2D, right).

Reduced CAPRIN1 protein levels were also observed (Supplementary Fig. 3A).

Overall, CAPRIN1 protein levels were clearly reduced in all samples analysed, supporting haploinsufficiency as the disease mechanism. This finding is in line with the type of mutations found in the cases and the high probability of intolerance to heterozygous LoF variation (pLI) from gnomAD (https://gnomad.broadinstitute.org).[31]

CAPRIN1 loss impairs neuronal structure organization and processes length

To analyse the impact of *CAPRIN1* haploinsufficiency in human neuronal cells, we generated an isogenic *CAPRIN1*$^{+/-}$ hiPSC line using the wild-type HUVEC hiPSC line and CRISPR–Cas9 technology[14] (Supplementary Fig. 4A and B). *CAPRIN1*$^{+/-}$ hiPSCs were differentiated into cortical neurons, using established protocols[16,32] with some modifications (Supplementary Fig. 4C). CAPRIN1 was well expressed in neuronal rosettes and in late cortical progenitors, and no significant differences in size were observed in *CAPRIN1*$^{+/-}$ neuronal rosettes compared to control (Fig. 3A and Supplementary Fig. 5A). No morphological alterations were observed in neural progenitor cells in further passages either (Supplementary Fig. 5B). In control neurons, CAPRIN1 localizes predominantly in the soma in immature stages and is then increasingly expressed in dendrites during development (Supplementary Fig. 6). *CAPRIN1*$^{+/-}$ immature neurons showed an alteration of neuronal structure, accompanied by reduced neurites length (Fig. 3B and C). This is consistent with previous observations suggesting a reduction in dendrite length and neuronal connectivity in murine *Caprin1*$^{-/-}$ primary embryonic neurons.[2]

Increased neuronal degeneration, calcium signal and reactive oxygen species in *CAPRIN1*$^{+/-}$ neurons

During time-course analysis of ND, we observed a progressive degeneration of neuronal processes in *CAPRIN1*$^{+/-}$ neurons, which began with the formation of small clusters of shrinking neuronal cells[33] between Days 17 and 19 post-ND in five independent cultures (Fig. 3D and Supplementary Fig. 7A). To understand the mechanisms behind this cellular phenotype, we investigated the possibility of calcium signal alterations. Impaired Ca^{2+} homeostasis and overload have been described as triggering or contributing to neuronal cell death.[34–36] Using a fluorescent tracer, we recorded Ca^{2+} signals in neurons 10 and 14 days post-ND, using live imaging (Supplementary Video 4). We chose these time points before cell death to minimize confounding factors and to study events leading to neuronal degeneration. Recordings for 2 min under controlled CO_2 and temperature conditions showed an increase in Ca^{2+} signals in *CAPRIN1*$^{+/-}$ compared to control neurons, both at 10 and 14 days post-ND (Fig. 4A).

Neuronal death has also been attributed to the induction of ROS.[37] Thus, we tested whether the elevated Ca^{2+} levels could contribute to ROS induction.[38,39] We analysed neurons 18 days post-ND, to capture the events immediately before neuronal death. Cells were treated with CellROX™ for 30 min and then fixed and counterstained with DAPI for immunofluorescence analysis. Notably, we observed a significant increase in CellROX signal in

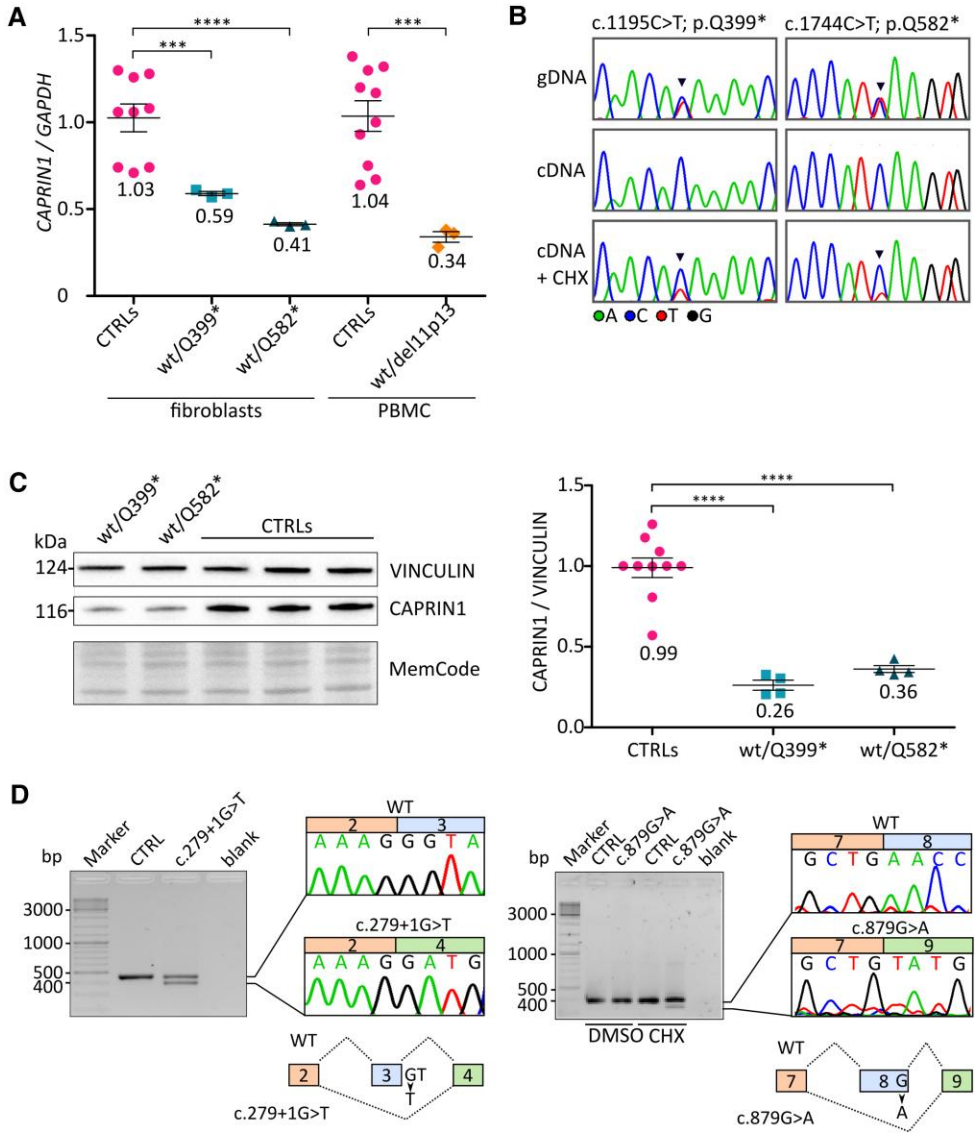

Figure 2 Expression analysis of *CAPRIN1* in patient-derived cells. (**A**) Expression of *CAPRIN1* versus *GAPDH* was reduced in patients' fibroblasts or PBMC, measured by RT-qPCR (Case 8, wt/Gln399Ter (in figure Q399*) = 0.59 ± 0.01, $n = 3$; Case 12, wt/Gln582Ter (in figure Q582*) = 0.41 ± 0.01, $n = 3$; CTRLs = 1.03 ± 0.08, $n = 9$; Case 1, wt/del11p13 = 0.34 ± 0.03, $n = 9$ CTRLs = 1.04 ± 0.09, $n = 3$; mean ± SEM. $P = 0.0007$ (Q399* versus CTRLs) and <0.0001 (Q582* versus CTRLs and del11p13 versus CTRLs). For each experiment, three different controls were used, and the experiments were performed in triplicate; controls were healthy young adults. (**B**) Sanger sequencing of the cDNA containing the c.1195C>T p.Gln399Ter and c.1744C>T p.Gln582Ter shows that the mutant allele is probably degraded by NMD; cDNA panels. Indeed, treating cells with CHX, an NMD blocker, prior to RNA extraction, partially rescued the expression of the mutant allele (cDNA + CHX panels). As comparison, the sequences obtained from genomic DNA (gDNA panels). (**C**) CAPRIN1 protein analysis in fibroblasts of the patients carrying the c.1195C>T p.Gln399Ter and c.1744C>T p.Gln582Ter variants. Western blot shows a protein reduction compatible with a half dose (Case 8 = 0.26 ± 0.03, $n = 4$; Case 12 = 0.36 ± 0.02, $n = 4$; CTRLs = 0.99 ± 0.06, $n = 10$. $P <$ 0.0001). For every experiment, three controls were used from different healthy patients (young adults) and experiments were performed a minimum of three times. Vinculin was used as a normalizer, and MemCode stain (Thermo Fisher Scientific) to confirm the efficiency of protein transferring and the overall protein abundancy. (**D**) Analysis of the cDNA from LCLs of the c.279+1G>T (Case 2) and c.879G>A (Case 3) carriers. The c.279+1G>T change causes an in-frame 84 bp exon 3 skipping (*left*). The c.879G>A affects the last base of exon 8 and causes out-of-frame skipping of exon 8 and a degradation by NMD. Exon 8 skipping could be detected by CHX treatment (*right*). Control (CTRL) LCLs derived from a young adult sex-matched healthy patient.

CAPRIN1$^{+/-}$ cells compared to controls (Fig. 4B), confirming an increase in ROS after Ca^{2+} overload.

Loss of CAPRIN1 causes an increased global mRNA translation in neurons

CAPRIN1 has been suggested to be a translational inhibitor, and its overexpression results in global reduction of protein synthesis in HeLa cells.[40] Interestingly, CAPRIN1 interacts with other proteins involved in neurodevelopment, including FMRP[6] and the cytoplasmic FMRP-interacting protein 1 (CYFIP1),[41] both of which are involved in the regulation of mRNA translation and formation of dendritic spines.[41,42]

Protein synthesis is tightly regulated in neurons, with spatial and temporal regulation of gene expression.[43] To understand whether a lack of CAPRIN1 causes an increase of protein synthesis,

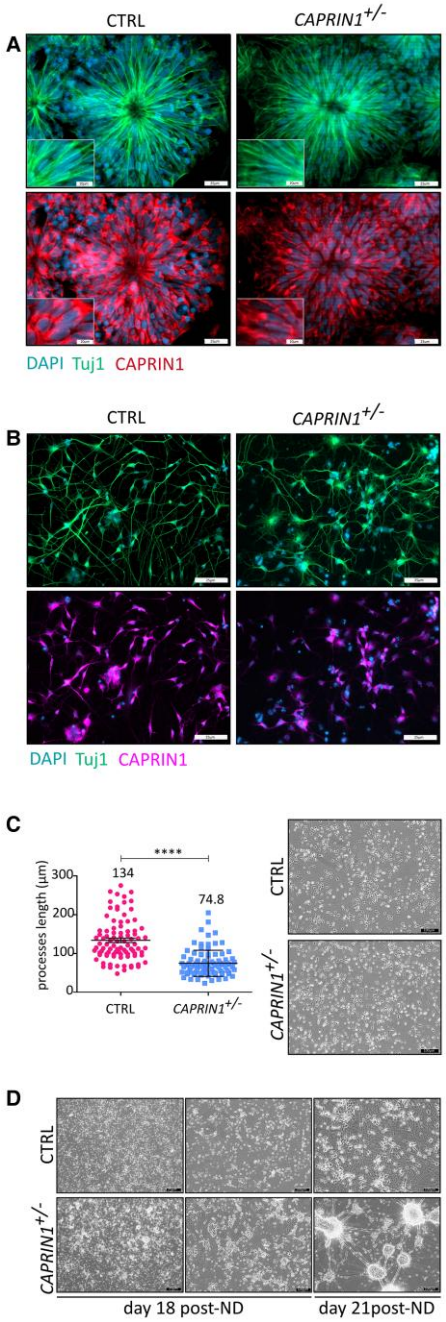

Figure 3 Haploinsufficiency of *CAPRIN1* causes impaired neuronal organization and increased degeneration of neuronal processes. (**A**) Representative images of neuronal rosettes derived from CTRL and *CAPRIN1*$^{+/-}$ cells. CAPRIN1 protein (magenta) could be easily detected in these structures. No gross morphological differences were observed between CTRL and *CAPRIN1*$^{+/-}$ rosettes. Images were acquired at ×40 magnification using Z-stack mode. The neuronal marker Tuj1 (green) is used to see the rosette morphology, and the DAPI (blue) to stain the nucleus. (**B**) *CAPRIN1*$^{+/-}$ neurons 10 days post-ND showed an impaired neuronal organization (×20 magnification; blue = DAPI; magenta = CAPRIN1; green = Tuj1. Scale bar = 25 µm). (**C**) Quantification of neuronal processes length on ×20 brightfield images, Day 7 post-ND. Length was quantified using the Fiji/ImageJ tool. CTRL = 134 ± 5.62, $n = 90$; *CAPRIN1*$^{+/-}$ = 74.8 ± 3.55, $n = 90$; mean ± SEM; $P < 0.0001$. Each dot represents a different neuronal process; images deriving from three independent differentiations were analysed. (**D**) Representative images of the neuronal death observed starting 18 days post-ND. Images were acquired 18 days post-ND (*left*: ×4 magnification, *middle*: ×10 magnification) and 21 days post-ND (*right*: ×20 magnification), using a brightfield microscope.

we performed the SUnSET assay. This method tests global protein synthesis on the basis of puromycin incorporation and is commonly used to measure relative rates of *de novo* protein synthesis.[19] Treatment of hiPSCs-derived neurons with 1 µg/ml puromycin for 30 min resulted in a slightly increased global translation in *CAPRIN1*$^{+/-}$ neurons 4 days post-ND ($P = 0.228$) (Supplementary Fig. 8A), which became significantly higher 14 days post-ND ($P = 0.03$) (Fig. 5A).

Interestingly, a difference in the distribution of the puromycin signal along the neurons was also observed (Fig. 5B and C), both 4 and 10 days post-ND. In control neurons, the signal was higher near the soma and then slowly decreased along the dendrite; similarly, *CAPRIN1*$^{+/-}$ cells showed higher puromycin fluorescence intensity the cell body, which decreased rapidly in the dendrite starting at ~5 µm from the soma, much more intense than in controls. These data suggest that *CAPRIN1* haploinsufficiency might also affect local protein synthesis.

CAPRIN1$^{+/-}$ neurons display abnormal spontaneous firing properties

In *Caprin1*$^{+/-}$ mice, neurons had a reduced firing activity.[3] To investigate whether the impaired neuronal structure organization affects network activity during neuronal maturation also in human *CAPRIN1*$^{+/-}$ neurons, we compared the electrical properties of *CAPRIN1*$^{+/-}$ hiPSC-derived neurons and controls using microelectrode arrays (MEAs).[16,17] Spontaneous firing of neurons was monitored from Day 0 to Day 14 post-ND to assess stages of network maturation (Fig. 6A). Both control and *CAPRIN1*$^{+/-}$ neurons showed firing properties already at 4 days post-ND. The spike rate and spike count were significantly lower in *CAPRIN1*$^{+/-}$ neurons versus controls, both at immature (post-ND Days 4 and 7) and more mature stages (post-ND Days 10 and 14) (Fig. 6B and C). In addition, the burst count 10 and 14 days post-ND, was significantly lower in *CAPRIN1*$^{+/-}$ neurons, with the absence of bursts in most of the wells. Interestingly, the duration of the detected bursts was also shorter in *CAPRIN1*$^{+/-}$ neurons compared to controls (Fig. 6D and E).

Overall, these results confirmed a reduced spontaneous activity (spike rate and count) and decreased synchronization of *CAPRIN1*$^{+/-}$ neurons (burst count).

Discussion

CAPRIN1 is a candidate gene for ASD (high confidence SFARI 1; https://gene.sfari.org/): a *de novo* nonsense variant was identified in a male ASD proband[11] and, more recently, a second nonsense *CAPRIN1* variant was found in a genome sequencing screening of families with multiple ASD-affected children.[10] In a recent combined analysis of 33 different ASD cohorts,[12] *CAPRIN1* was identified as a risk genes associated with ASD and NDDs.[12] However, a causal relation between the gene and neurodevelopmental disorders was still missing. Our work provides the first clinical characterization of the individuals with *CAPRIN1* haploinsufficiency and supports a key role for *CAPRIN1* in human neuronal development and activity.

Our data point to a critical role of CAPRIN1 in neuronal morphogenesis and survival. *CAPRIN1*$^{+/-}$ hiPSC-derived neurons have aberrant neuronal organization, reduced length of neuronal processes, progressive neuronal degeneration and premature cell death beginning 17–19 days post-ND. In *Caprin1*$^{-/-}$ cortical neurons, the length and number of dendrites and the formation of neuronal networks were reduced compared to wild-type. Interestingly, network area

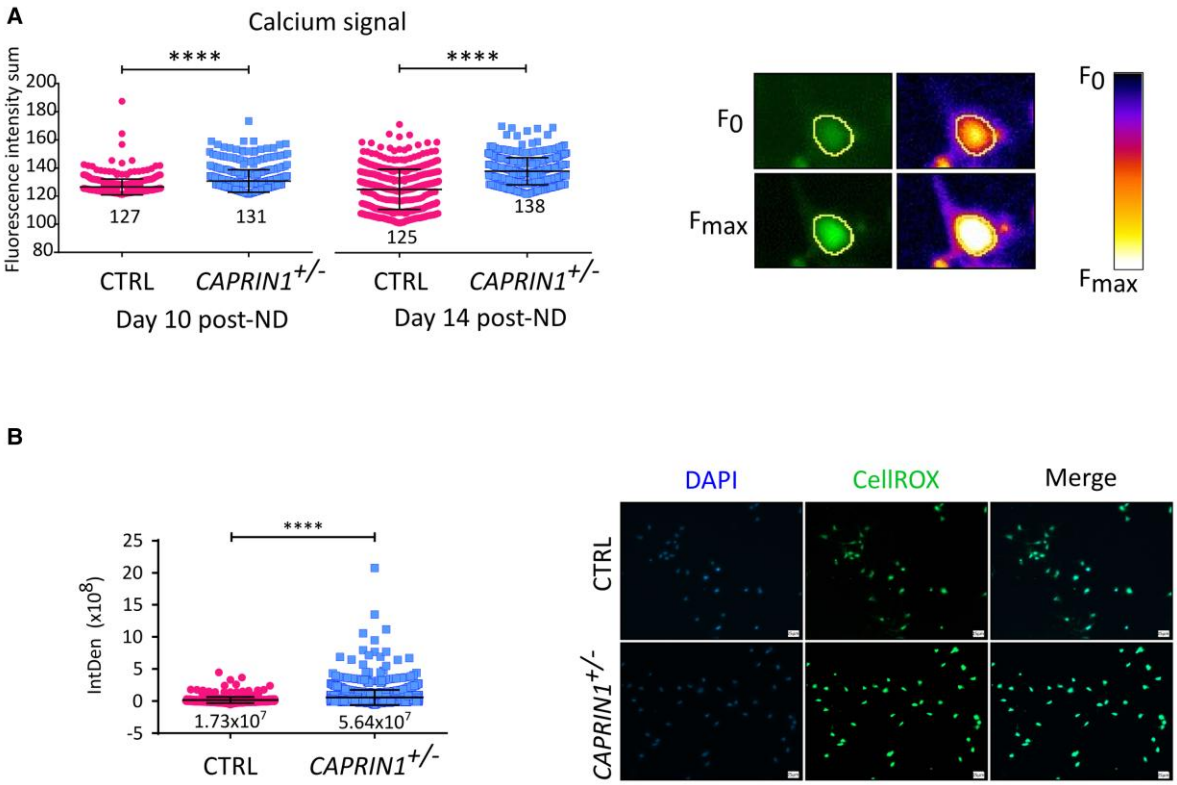

Figure 4 Calcium overload and increased oxidative stress are observed in *CAPRIN1*$^{+/-}$ neurons. (**A**) Quantification of calcium signal in *CAPRIN1*$^{+/-}$ neurons 10 and 14 days post-ND. Neurons were recorded for 2 min, and the integrated density (IntDen) signal of each cell was normalized on its lowest value during this time. *Right*: A representative image of the lowest (F_0) and maximum (F_{max}) fluorescence intensity for each cell; the lookup table 'fire' was used. *Left*: The Fluo-4 (green) signal, more appreciable in the image on the *right* (Day 10 post-ND: CTRL = 127 ± 0.25, n = 197; *CAPRIN1*$^{+/-}$ = 131 ± 0.37, n = 197; Day 14 post-ND: CTRL = 125 ± 0.67, n = 354; *CAPRIN1*$^{+/-}$ = 138 ± 0.45, n = 361; $P < 0.0001$). For every genotype and time point, three different coverslips were analysed, each of them deriving from an independent differentiation. (**B**) Analysis of *CAPRIN1*$^{+/-}$ neurons (Day 18 post-ND) with CellROX showed a significant increase of ROS (CTRL = $1.73 \times 10^7 \pm 1.80 \times 10^6$, n = 697; *CAPRIN1*$^{+/-}$ = $5.64 \times 10^7 \pm 2.96 \times 10^6$, n = 1596; $P < 0.0001$). Twenty-two images for every genotype have been analysed from three different coverslips, each of them deriving from an independent differentiation. *Right*: Example of the difference between CTRL and *CAPRIN1*$^{+/-}$ neurons (×20 magnification; blue = DAPI; green = CellROX. Scale bar = 25 µm).

was always smaller compared to wild-type neurons, but it degenerated during neuronal maturation, particularly after 22 days *in vitro* (DIV).[2] Similarly, in our cell model, we observed an aberrant neuronal organization and reduced length of neuronal processes (Fig. 3B and C). In the mouse model, the lack of *Caprin1* caused increased cell death both *in vitro*—in cortical neurons from 10 DIV—and *in vivo*, as demonstrated by an increased cleaved caspase-3 signals in brain slices.[2]

One of the proposed mechanisms for these cellular phenotypes is decreased of Na^+/K^+ ATPase (NKA) activity.[2] Inhibition of NKA activity results in increased sensitivity to glutamate excitotoxicity, which subsequently causes an increase of intracellular Na^+ and Ca^{2+} ions.[44] In addition, inhibition of NKA can partially suppress excitatory postsynaptic potentials (EPSPs) and reduce surface concentrations of AMPA receptors in neurons.[45] In *CAPRIN1*$^{+/-}$ human neurons, we observed a Ca^{2+} overload 10 and 14 days post-ND and an overall reducing firing rate and synchronization on neuronal activity. In the mouse model, heterozygous loss of *CAPRIN1* causes reduced amplitude and slope of field EPSPs in hippocampal slices.[4] Altogether, our data and published data support the hypothesis that previously reported impairment of NKA activity[2] affects Ca^{2+} homeostasis and electrical activity in *CAPRIN1*$^{+/-}$ neurons.

Further, during mouse cortical development CAPRIN1 interacts with several mRNAs, including some metal-binding proteins as selenoprotein W and metallothionein 2, involved in protection against ROS.[2] In *CAPRIN1*$^{+/-}$ hiPSC-derived neurons, we observed a significant increase in ROS production concomitant with the neuronal cell degeneration 18 days post-ND. The link between ROS, ASD and ADHD has been reported in the literature, and some therapies are now focusing on antioxidant drugs.[46] Also, diagnostic biomarkers investigating redox metabolism, are the subject of study in patients with ASD and ADHD, as for instance total, oxidized and free reduced glutathione levels[47] or thiol/disulphide homeostasis.[48] It will be of interest to further study increased ROS species in *CAPRIN1*$^{+/-}$ neurons, as the method used in the present work detected a global ROS signal but did not discriminate between different ROS types.[37]

Another potential CAPRIN1 target that might mediate the cellular phenotypes we observe is the Defender against apoptotic cell death (DAD1), a cell death suppressor that may act downstream of the BCL-2 protein[49]; in a microarray analysis of CAPRIN1-bound mRNAs, DAD1 has been identified as an interactor.[2]

Non-neuronal cells lacking *CAPRIN1* do not exhibit changes in global rate of protein synthesis,[7] whereas the local expression of some mRNAs have been reported as altered in a conditional model

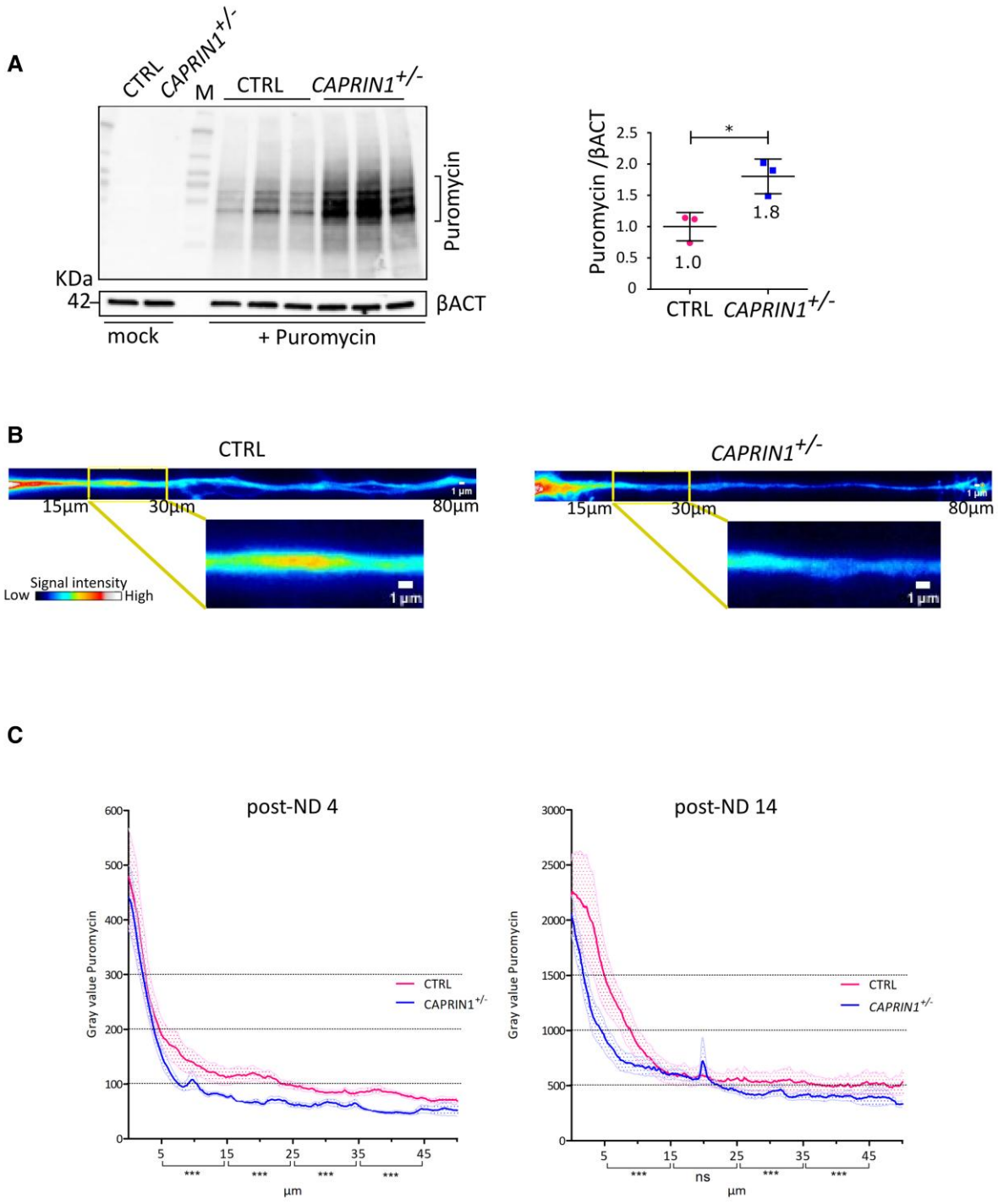

Figure 5 *CAPRIN1*$^{+/-}$ neurons show increased global translation and slight alteration of local translation. (**A**) Western blot analysis of SUnSET assay on neurons 14 days post-ND treated with 1 µM puromycin for 30 min showed a significantly higher puromycin signal compared to CTRL. Each CTRLs and *CAPRIN1*$^{+/-}$ lane (and dot on the graph) represents an independent ND ($n = 3$). (**B**) Immunofluorescence analysis of SUnSET assay on *CAPRIN1*$^{+/-}$ neurons 4 days post-ND, treated with 1 µM puromycin for 30 min. Representative images for CTRL and *CAPRIN1*$^{+/-}$ dendrites are reported (4 days post-ND, zoom of ×40 magnification, scale bar = 1 µm), using the ImageJ/Fiji lookup table 'royal', to visualize the strength of the signal better.[57] Magnification of the dendrites show the puromycin fluorescence intensity from 0 to 80 µm of distance from the cell bodies; intensity of signal is maintained along the dendrite in CTRL neurons, while it decreases visibly in *CAPRIN1*$^{+/-}$ ones. Enlarged views of the fragment from 15 to 30 µm of the dendrite are provided below (scale bar = 1 µm), showing reduced intensity of signal in *CAPRIN1*$^{+/-}$ neurons. An image of the entire neuron is provided in Supplementary Fig. 8C. (**C**) Quantification of the puromycin signal, indicated as grey value, along the dendrite ($n = 6$). Both panels (*left* = 4 days post-ND; *right* = 14 days post-ND) show higher signal in proximity of the soma, that progressively decrease. However, the decrease is significantly higher in *CAPRIN1*$^{+/-}$ neurons, particularly 4 days post-ND. Statistical significance was tested by two-way ANOVA followed by Bonferroni *post hoc* tests; column factor was considered. *P*-value < 0.0001; mean and error (SEM) are shown.

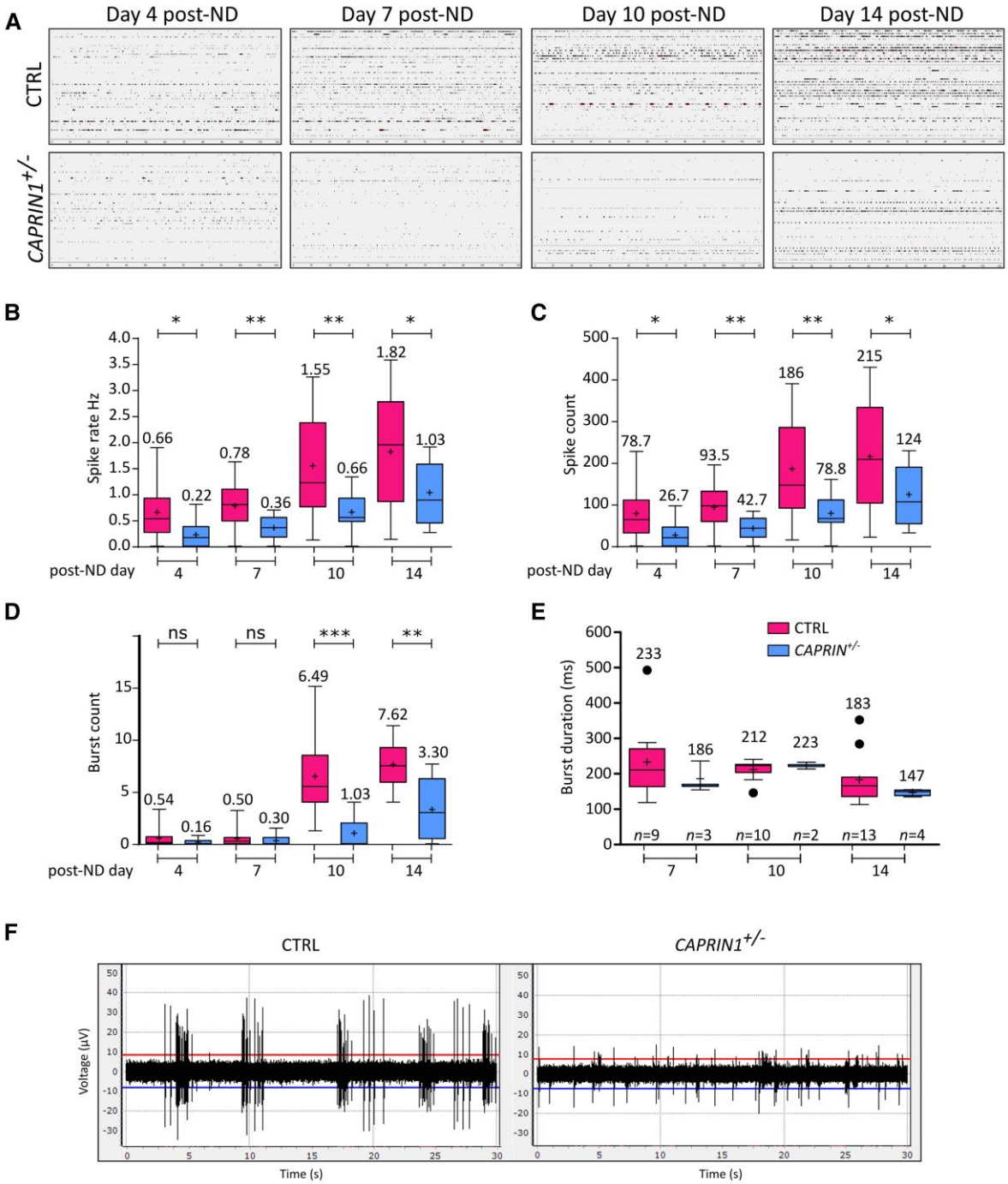

Figure 6 Neurons deficient for *CAPRIN1* show abnormal firing properties. (**A**) MEA analyses in CTRL and *CAPRIN1*$^{+/-}$ neurons at different stages of maturation (Days 4, 7, 10 and 14 post-ND). Each image is representative of three different wells, recorded for 2 min on 12 electrodes. Box and whisker plots (5–95th percentile), outliers are indicated as dots; mean is indicated with a plus symbol; numbers on each bar indicate the mean. Wells that never showed an activity throughout the time course have been excluded from the analysis (total CTRL $n = 14$ wells; total *CAPRIN1*$^{+/-}$ $n = 9$ wells). (**B**) Quantification of MEA data, reporting the spike rate (Hz) along the 2 min of recording (Day 4 CTRL = 0.66 ± 0.14; *CAPRIN1*$^{+/-}$ = 0.22 ± 0.09; mean ± SEM; $P = 0.02$; Day 7 CTRL = 0.78 ± 0.11; *CAPRIN1*$^{+/-}$ = 0.36 ± 0.08; $P = 0.006$; Day 10 CTRL = 1.55 ± 0.28; *CAPRIN1*$^{+/-}$ = 0.66 ± 0.13; $P = 0.01$; Day 14 CTRL = 1.82 ± 0.29; *CAPRIN1*$^{+/-}$ = 1.03 ± 0.20; $P = 0.04$). (**C**) Quantification of MEA data, reporting the spikes count along the 2 min of recording (Day 4 CTRL = 78.7 ± 17.3; *CAPRIN1*$^{+/-}$ = 26.7 ± 10.9; mean ± SEM; $P = 0.02$; Day 7 CTRL = 93.5 ± 13.6; *CAPRIN1*$^{+/-}$ = 42.7 ± 9.06; $P = 0.006$; Day 10 CTRL = 186 ± 33.3; *CAPRIN1*$^{+/-}$ = 78.8 ± 15.7; $P = 0.01$; Day 14 CTRL = 215 ± 35.3; *CAPRIN1*$^{+/-}$ = 124 ± 24.3; $P = 0.05$). (**D**) Burst count along the 2 min of recording (Day 4 CTRL = 0.54 ± 0.25; *CAPRIN1*$^{+/-}$ = 0.16 ± 0.10; mean ± SEM; $P = 0.18$; Day 7 CTRL = 0.50 ± 0.22; *CAPRIN1*$^{+/-}$ = 0.30 ± 0.17; $P = 0.48$; Day 10 CTRL = 6.49 ± 1.05; *CAPRIN1*$^{+/-}$ = 1.03 ± 0.47; $P = 0.002$; Day 14 CTRL = 7.62 ± 0.64; *CAPRIN1*$^{+/-}$ = 3.30 ± 0.98; $P = 0.002$). (**E**) Burst duration (ms) along the 2 min of recording (Day 7 CTRL = 233 ± 36.7; *CAPRIN1*$^{+/-}$ = 186 ± 25.3; Day 10 CTRL = 212 ± 8.76; *CAPRIN1*$^{+/-}$ = 223 ± 9.51; Day 14 CTRL = 183 ± 18.5; *CAPRIN1*$^{+/-}$ = 147 ± 4.49). The number of bursts in CTRL was higher compared to *CAPRIN1*$^{+/-}$, therefore the number of considered events (n) is reported. (**F**) Representative images of CTRL and *CAPRIN1*$^{+/-}$ detected spikes.

of *Caprin1* knock-out mouse.[4] In our work, we showed that *CAPRIN1* haploinsufficiency is sufficient to cause a significant increase of global translation in neuronal cells (Fig. 5A) and an impairment of its localization (Fig. 5B and C), enforcing the concept that the use of the right cellular model is important to detect cell-specific phenomena. Interestingly, it has been shown CAPRIN1 selectively targets dendritic mRNAs, and an increase in mRNAs in soma but a decrease in mRNAs in dendrites has been observed in *Caprin1* conditional knock-out neurons.[4] This further supports the decrease in local translation in distal dendrites in *CAPRIN1*$^{+/-}$ neurons that we identified (Fig. 5B and C). A rapid response to physiological and pathological mechanisms adjusting the protein synthesis rate is also mediated by oxidative stress.[46] Both the administration of H_2O_2 and the endogenous increase of ROS can reduce cytosolic protein synthesis in a reversible manner.[50,51] It is therefore possible that the increased oxidative stress we observed is an attempt by the neuron to balance the increased translational rate caused by *CAPRIN1* loss.

The lack of impact on global translation in a non-neuronal cell line[7] suggests the loss of *CAPRIN1* can have different outcomes depending on the cell type, explaining the predominantly neurological phenotypes we observed in our patients despite the ubiquitous expression of *CAPRIN1* in human tissues.

In our patients, we reported ASD in 67% of cases, and this clinical phenotype is compatible with the reduced sociability and weaker preference for social novelty previously observed in *Caprin1*$^{+/-}$ mice.[3] We observed intellectual or learning disability in 83% of cases; *Caprin1*$^{+/-}$ mice have difficulties in reversal learning, but no overall memory deficits.[3] However, a *Caprin1* brain conditional knock-out model shows a deficit in spatial and fear conditioning long-term memory, as well as reduced basal and induced synaptic transmission in hippocampal neurons.[4] One-third of our patients showed seizures with variable presentation. Interestingly, seizures were sporadically noted in *Caprin1* mutant mice during and after the Morris water maze and contextual fear conditioning tests, and epileptic-like fEPSP were recorded after induction of long-term potentiation.[4] These data suggest that the epileptic phenotype could be triggered by specific events. We also noted six cases with respiratory problems, a finding consistent with the post-natal failures in breathing in the *Caprin1*$^{-/-}$ mouse model.[2]

Caprin1 has recently been associated with early onset progressive hearing loss and reduced protection from noise exposure in an inner ear conditional knock-out mouse.[29] We found a clinical report of mild hearing loss in in a paediatric (Case 3) and an adult case (Case 10). The adult case works in an environment with high exposure to loud sounds, which is associated with increased risk for hearing loss,[52] supporting the data that lack of *Caprin1* is involved in recovery from audible insults.[29] It is possible that most of the affected individuals do not show hearing impairment due to the young age, but they might develop this phenotype in the future.

Despite the ubiquitous expression of *CAPRIN1* in humans, we observed prevalently neurological features; however, some minor and variable defects at the level of skeletal, respiratory, visual and auditory systems were identified. Noteworthy, the association between diseases and affected tissues is not always straightforward and it is common in genetic disorders to observe the impairment of only a small portion of tissues compared to the broader expression of the causal gene.[53] This could be explained by several mechanisms, including disrupted pathways, regulatory elements, post-transcriptional mechanisms and microenvironment that can be cell- or tissue-specific.[53] Observations of *Caprin1* heterozygous, homozygous or conditional mutants suggest impairment of the auditory[29] and respiratory[54] systems, but there is no evidence for skeletal or ocular involvement. Non-neurological features are observed only in a fraction of patients. We cannot, therefore, exclude the presence of intra- or extragenic eQTLs or single-nucleotide polymorphisms that contribute to the variable presentation of those phenotypes.

Variants identified in our cases were heterozygous LoF because they introduced a premature stop codon by changing an amino acid, introducing a frameshift or altering splicing.[6]

Ten cases were *de novo*, and two familial (Supplementary Fig. 1). Case 9 and his father (Case 10) carried the p.(Arg458Ter) variant. Both showed language delay, ADHD and mild intellectual disability/developmental delay as children, but the father had recovered most of his language impairments by adulthood. Case 2 had the c.279+1G>T variant inherited from his mother, reported healthy and without history of intellectual disability, speech delay, neurodevelopmental/behavioural concerns or other medical issues; she had a college education. These cases suggest the disease has a variable expressivity during life and/or incomplete penetrance; it is also tempting to speculate a sex bias, given the healthy female carrier and the observation that nine out of 12 affected individuals were males.

Our work focused on *CAPRIN1* LoF variants (nonsense, splicing and small copy number variants). The possibility that missense variants are also associated with CAPRIN1-NDD is still to be explored. Overall, *CAPRIN1* is not anticipated to be highly sensitive to missense variations (Z-score = 1.69, GnomAD)[26]; however, some specific regions of the protein are predicted to be intolerant or highly intolerant to changes, according to MetaDome server (v1, https://stuart.radboudumc.nl/metadome).[55] Intolerant amino acids are predominantly located between amino acids 58–131 and 514–583, part of the Homologous Regions 1 and 2 (HR1 and HR2) domains of CAPRIN1.[6] Indeed, a p.(Pro512Leu) recurrent missense variant in the HR2 domain has been recently found in two independent patients with a neurodegenerative syndrome with ataxia.[58] This indicates that different neurological phenotypes are associated with *CAPRIN1*, depending on the variant and its pathophysiological significance. The future inclusion of *CAPRIN1* in diagnostic genetic panels might help identifying cases with missense variants and will probably expand the clinical spectrum associated with the gene.

Altogether, our data finally link *CAPRIN1* haploinsufficiency with an autosomal dominant neurodevelopmental disorder, characterized by language impairment, ADHD, intellectual or learning disability and ASD, with other variably associated features including respiratory, skeletal, ocular, auditory and gastrointestinal issues. Likewise, *CAPRIN1* haploinsufficiency damaged the overall organization of hiPSC-derived neurons, and mediated impairment of Ca^{2+} homeostasis, neuronal activity, ROS production and global translation rate.

Acknowledgements

The authors wish to acknowledge the resources of MSSNG (www.mss.ng), Autism Speaks and The Centre for Applied Genomics at The Hospital for Sick Children, Toronto, Canada. We also thank the participating families for their time and contributions to this database, as well as the generosity of the donors who supported this programme. We are grateful to the patients and their family for their collaboration. We are grateful to L. Kurian, CMMC for providing us the Cas9-expressing vector pX330-hCas9-long-chimeric-grna-g 2p. L.P.'s work was supported by a Deutscher Akademischer Austauschdienst (DAAD) research grant for doctoral students

(www.daad.de) and we are thankful for this support. S.D.R. is supported by the Beatrice and Samuel A. Seaver Foundation.

Funding

This research received funding specifically appointed to Department of Medical Sciences (University of Turin) from the Italian Ministry for Education, University and Research (Ministero dell'Istruzione, dell'Università e della Ricerca—MIUR) under the programme 'Dipartimenti di Eccellenza 2018–2022' Project code D15D18000410001. We thank the support of 'Associazione Emma ed Ernesto Rulfo per la Genetica Medica' and Fondazione Cassa di Risparmio Torino to A.B. Research to B.W. was supported by the Deutsche Forschungsgemeinschaft [Wi 945/17-1 (project ID 398410809); Wi 945/18-1 (project ID 384170921); Wi 945/19-1 (project ID 417989143); SFB1451 (project ID 431549029—A01), and GRK1960 (project ID 233886668)], the European Research Council (ERC) under the HORIZON EUROPE European Research Council 2020 and HORIZON EUROPE Marie Sklodowska-Curie Actions 2020 (956185: SMABEYOND) and Center for Molecular Medicine Cologne (project no. C18). E.A. and D.C. were supported by Ricerca Corrente 2021, Ministero della Salute. D.C. was supported by MSALRC21 (Ministero Salute Ricerca Corrente) and ALBURLORF, DLDG514/20 (Progetto Ricerca collaborativo Rete IRCCS IDE). The collection of some of the samples was supported by the National Institute of Mental Health NIMH (U01MH111661 to J.D.B.). Two authors of this publication are members of the European Reference Network for rare malformation syndromes and rare intellectual and neurodevelopmental disorders, ERN-ITHACA.

Competing interests

S.W.S. is on the Scientific Advisory Committees of Population Bio and Deep Genomics, serves as a Highly Cited Academic Advisor for the King Abdulaziz University, and intellectual property from aspects of his research held at the Hospital for Sick Children are licensed to Athena Diagnostics and Population Bio.

Supplementary material

Supplementary material is available at *Brain* online.

References

1. Yang ZS, Qing H, Gui H, Luo J, Dai LJ, Wang B. Role of caprin-1 in carcinogenesis (Review). *Oncol Lett*. 2019;18:15–21.
2. Shiina N, Yamaguchi K, Tokunaga M. RNG105 Deficiency impairs the dendritic localization of mRNAs for Na+/K+ ATPase subunit isoforms and leads to the degeneration of neuronal networks. *J Neurosci*. 2010;30:12816–12830.
3. Ohashi R, Takao K, Miyakawa T, Shiina N. Comprehensive behavioral analysis of RNG105 (Caprin1) heterozygous mice: Reduced social interaction and attenuated response to novelty. *Sci Rep*. 2016;6:20775.
4. Nakayama K, Ohashi R, Shinoda Y, *et al*. RNG105/caprin1. An RNA granule protein for dendritic mRNA localization, is essential for long-term memory formation. *eLife*. 2017;6:1–32.
5. El Fatimy R, Tremblay S, Dury AY, *et al*. Fragile mental retardation protein interacts with the RNA-binding protein Caprin1 in neuronal ribonucleoprotein complexes [corrected]. *PLoS ONE*. 2012;7:e39338.
6. Wu Y, Zhu J, Huang X, Du Z. Crystal structure of a dimerization domain of human caprin-1: Insights into the assembly of an evolutionarily conserved ribonucleoprotein complex consisting of caprin-1, FMRP and G3BP1. *Acta Crystallogr D Struct Biol*. 2016;72:718–727.
7. Solomon S, Xu Y, Wang B, *et al*. Distinct structural features of caprin-1 mediate its interaction with G3BP-1 and its induction of phosphorylation of eukaryotic translation InitiationFactor 2α, entry to cytoplasmic stress granules, and selective interaction with a subset of mRNAs. *Mol Cell Biol*. 2007;27:2324–2342.
8. Shiina N, Shinkura K, Tokunaga M. A novel RNA-binding protein in neuronal RNA granules: Regulatory machinery for local translation. *J Neurosc*. 2005;25:4420–4434.
9. Solomon S, Xu Y, Wang B, *et al*. Distinct structural features of Caprin-1 mediate its interaction with G3BP-1 and its induction of phosphorylation of eukaryotic translation initiation factor 2α, entry to cytoplasmic stress granules, and selective interaction with a subset of mRNAs. *Mol Cell Biol*. 2007;27:2324–2342.
10. Ruzzo EK, Pérez-Cano L, Jung JY, *et al*. Inherited and De Novo genetic risk for autism impacts shared networks. *Cell*. 2019;178:850–866.e26.
11. Deciphering Developmental Disorders Study. Prevalence and architecture of de novo mutations in developmental disorders. *Nature*. 2017;542:433–438.
12. Fu JM, Satterstrom FK, Peng M, *et al*. Rare coding variation illuminates the allelic architecture, risk genes, cellular expression patterns, and phenotypic context of autism. *Nat Genet*. 2022;54:1320–1331.
13. Li Q, Wang K. Intervar: Clinical interpretation of genetic variants by the 2015 ACMG-AMP guidelines. *Am J Hum Genet*. 2017;100:267–280.
14. Panopoulos AD, Ruiz S, Yi F, *et al*.. Rapid and highly efficient generation of induced pluripotent stem cells from human umbilical vein endothelial cells. *PLoS ONE*. 2011;6:e19743.
15. Frank S, Ahuja G, Bartsch D, *et al*. Yylnct defines a class of divergently transcribed lncRNAs and safeguards the T-mediated mesodermal commitment of human PSCs. *Cell Stem Cell*. 2019;24:318–327.e8.
16. Boissart C, Poulet A, Georges P, *et al*. Differentiation from human pluripotent stem cells of cortical neurons of the superficial layers amenable to psychiatric disease modeling and high-throughput drug screening. *Transl Psychiatry*. 2013;3:e294.
17. Darville H, Poulet A, Rodet-Amsellem F, *et al*. Human pluripotent stem cell-derived cortical neurons for high throughput medication screening in autism: A proof of concept study in SHANK3 haploinsufficiency syndrome. *EBioMedicine*. 2016;9:293–305.
18. Bachmann S, Linde J, Bell M, Spehr M, Zempel H, Zimmer-Bensch G. DNA Methyltransferase 1 (DNMT1) shapes neuronal activity of human iPSC-derived glutamatergic cortical neurons. *Int J Mol Sci*. 2021;22:2034.
19. Schmidt EK, Clavarino G, Ceppi M, Pierre P. SUnSET, a nonradioactive method to monitor protein synthesis. *Nat Methods*. 2009;6:275–277.
20. Kelley LA, Mezulis S, Yates CM, Wass MN, Sternberg MJE. The Phyre2 web portal for protein modeling, prediction and analysis. *Nat Protoc*. 2015;10:845–858.
21. Reynolds CR, Islam SA, Sternberg MJE. Ezmol: A web server wizard for the rapid visualization and image production of protein and nucleic acid structures. *J Mol Biol*. 2018;430:2244–2248.

22. Kozakov D, Beglov D, Bohnuud T, *et al*. How good is automated protein docking? *Proteins: Struct Funct Bioinf*. 2013;81:2159–2166.
23. Kozakov D, Hall DR, Xia B, *et al*. The ClusPro web server for protein–protein docking. *Nat Protoc*. 2017;12:255–278.
24. Vajda S, Yueh C, Beglov D, *et al*. New additions to the Cplus Pro server motivated by CAPRI. *Proteins*. 2017;85: 435–444.
25. Desta IT, Porter KA, Xia B, Kozakov D, Vajda S. Performance and its limits in rigid body protein-protein docking. *Structure*. 2020; 28:1071–1081.e3.
26. Lek M, Karczewski KJ, Minikel EV, *et al*. Analysis of protein-coding genetic variation in 60,706 humans. *Nature*. 2016;536: 285–291.
27. Sobreira N, Schiettecatte F, Valle D, Hamosh A. Genematcher: A matching tool for connecting investigators with an interest in the same gene. *Hum Mutat*. 2015;36:928–930.
28. Richards S, Aziz N, Bale S, *et al*. Standards and guidelines for the interpretation of sequence variants: A joint consensus recommendation of the American college of medical genetics and genomics and the association for molecular pathology. *Genet Med*. 2015;17:405–424.
29. Nolan LS, Chen J, Gonçalves AC, *et al*. Targeted deletion of the RNA-binding protein Caprin1 leads to progressive hearing loss and impairs recovery from noise exposure in mice. *Sci Rep*. 2022;12:2444.
30. Sauna ZE, Kimchi-Sarfaty C. Understanding the contribution of synonymous mutations to human disease. *Nat Rev Genet*. 2011; 12:683–691.
31. Karczewski KJ, Francioli LC, Tiao G, *et al*. The mutational constraint spectrum quantified from variation in 141,456 humans. *Nature*. 2020;581:434–443.
32. Chailangkarn T, Trujillo CA, Freitas BC, *et al*. A human neurodevelopmental model for Williams syndrome. *Nature*. 2016;536: 338–343.
33. Moujalled D, Strasser A, Liddell JR. Molecular mechanisms of cell death in neurological diseases. *Cell Death Differ*. 2021;28: 2029–2044.
34. Calvo M, Villalobos C, Núñez L. Calcium imaging in neuron cell death. *Methods Mol Biol*. 2015;1254:73–85.
35. Demaurex N, Distelhorst C. Cell biology. Apoptosis—The calcium connection. *Science*. 2003;300:65–67.
36. Mincheva-Tasheva S, Obis E, Tamarit J, Ros J. Apoptotic cell death and altered calcium homeostasis caused by frataxin depletion in dorsal root ganglia neurons can be prevented by BH4 domain of bcl-xL protein. *Hum Mol Genet*. 2014;23:1829–1841.
37. Sies H, Jones DP. Reactive oxygen species (ROS) as pleiotropic physiological signalling agents. *Nat Rev Mol Cell Biol*. 2020;21: 363–383.
38. Xu B, Chen S, Luo Y, *et al*. Calcium signaling is involved in cadmium-induced neuronal apoptosis via induction of reactive oxygen species and activation of MAPK/mTOR network. *PLoS One*. 2011;6:e19052.
39. Chen L, Xu B, Liu L, *et al*. Cadmium induction of reactive oxygen species activates the mTOR pathway, leading to neuronal cell death. *Free Radical Biol Med*. 2011;50:624632.
40. Solomon S, Xu Y, Wang B, *et al*. Distinct structural features ofCaprin-1 mediate its interaction with G3BP-1 and its induction of phosphorylation of eukaryotic translation InitiationFactor 2α, entry to cytoplasmic stress granules, and selective interaction with a subset of mRNAs. *Mol Cell Biol*. 2007;27:2324–2342.
41. De Rubeis S, Pasciuto E, Li KW, *et al*. CYFIP1 coordinates mRNA translation and cytoskeleton remodeling to ensure proper dendritic spine formation. *Neuron*. 2013;79:1169–1182.
42. Darnell JC, Klann E. The translation of translational control by FMRP: Therapeutic targets for FXS. *Nat Neurosci*. 2013;16:1530–1536.
43. Mofatteh M. mRNA localization and local translation in neurons. *AIMS Neurosci*. 2020;7:299–310.
44. Kinoshita PF, Orellana AMM, Nakao VW, *et al*. The Janus face of ouabain in Na^+/K^+-ATPase and calcium signalling in neurons. *Br J Pharmacol*. 2022;179:1512–1524.
45. Reich CG, Mason SE, Alger BE. Novel form of LTD induced by transient, partial inhibition of the Na, K-pump in rat hippocampal CA1 cells. *J Neurophysiol*. 2004;91:239–247.
46. Pangrazzi L, Balasco L, Bozzi Y. Oxidative stress and immune system dysfunction in autism spectrum disorders. *Int J Mol Sci*. 2020;21:3293.
47. Curpan AS, Luca AC, Ciobica A. Potential novel therapies for neurodevelopmental diseases targeting oxidative stress. *Oxid Med Cell Longevity*. 2021;2021:1–13.
48. Avcil S, Uysal P, Avcil M, Alışık M, Biçer C. Dynamic thiol/disulfide homeostasis in children with attention deficit hyperactivity disorder and its relation with disease subtypes. *Compr Psychiatry*. 2017;73:53–60.
49. Nakashima T, Sekiguchi T, Kuraoka A, *et al*. Molecular cloning of a human cDNA encoding a novel protein, DAD1, whose defect causes apoptotic cell death in hamster BHK21 cells. *Mol Cell Biol*. 1993;13:6367–6374.
50. Topf U, Suppanz I, Samluk L, *et al*. Quantitative proteomics identifies redox switches for global translation modulation by mitochondrially produced reactive oxygen species. *Nat Commun*. 2018;9:324.
51. Shenton D, Smirnova JB, Selley JN, *et al*. Global translational responses to oxidative stress impact upon multiple levels of protein synthesis. *J Biol Chem*. 2006;281:29011–29021.
52. Keithley EM. Pathology and mechanisms of cochlear aging. *J Neurosci Res*. 2020;98:1674–1684.
53. Hekselman I, Yeger-Lotem E. Mechanisms of tissue and cell-type specificity in heritable traits and diseases. *Nat Rev Genet*. 2020;21:137–150.
54. Shiina N, Yamaguchi K, Tokunaga M. RNG105 Deficiency impairs the dendritic localization of mRNAs for Na+/K+ ATPase subunit isoforms and leads to the degeneration of neuronal networks. *J Neurosci*. 2010;30:12816–12830.
55. Wiel L, Baakman C, Gilissen D, Veltman JA, Vriend G, Gilissen C. Metadome: Pathogenicity analysis of genetic variants through aggregation of homologous human protein domains. *Hum Mutat*. 2019;40:1030–1038.
56. Gurovich Y, Hanani Y, Bar O, *et al*. Identifying facial phenotypes of genetic disorders using deep learning. *Nat Med*. 2019;25:60–64.
57. Thelen MP, Wirth B, Kye MJ. Mitochondrial defects in the respiratory complex I contribute to impaired translational initiation via ROS and energy homeostasis in SMA motor neurons. *Acta Neuropathol Commun*. 2020;8:223.
58. Delle Vedove A, Natarajan J, Zanni G, *et al*. CAPRIN1 P512L causes aberrant protein aggregation and associates with early-onset ataxia. *Cell Mol Life Sci*. 2022;79(10):526.